Available online at www.sciencedirect.com
ScienceDirect
Cement and Concrete Research 37 (2007) 1206–1214
Cement and Concrete Research

Relation of expansion due to alkali silica reaction to the degree of reaction measured by SEM image analysis

M. Ben Haha, E. Gallucci *, A. Guidoum, K.L. Scrivener

Laboratory of Construction Materials, Ecole Polytechnique Fédérale de Lausanne, Switzerland

Received 4 January 2007; accepted 11 April 2007

Abstract

Scanning Electron Microscopy Image Analysis (SEM-IA) was used to quantify the degree of alkali silica reaction in affected microbars, mortar and concrete prisms. It was found that the degree of reaction gave a unique correlation with the macroscopic expansion for three different aggregates, stored at three temperatures and with two levels of alkali. The relationships found for the concretes and the mortars overlap when normalised by the aggregate content. This relationship seems to be linear up to a critical reaction degree which coincides with crack initiation within the reactive aggregates.

Keywords: Alkali–aggregate reaction; Backscattered Electron Imaging; Expansion; Degree of reaction

1. Introduction

The use of certain aggregates in concrete may result in a chemical process in which particular constituents of the aggregates react with alkali hydroxides present in the concrete pore solution. These alkali hydroxides originate mostly from the sodium and potassium ions in Portland cement, and occasionally from certain alkali-bearing rock materials. Amorphous or poorly crystalline silica in the aggregates is attacked by the alkali, forming a hydrous alkali-calcium-silica gel. The incorporation of water into this gel causes swelling, which leads to expansion and cracking of the concrete [1,2].

Although many studies have been made on the alkali silica reaction and methods are well established to avoid the occurrence of the reaction in new concrete, it remains difficult to establish the extent and future progress of the reaction in affected structures. This is particularly difficult in the case of slowly reacting aggregates where the manifestation of the reaction may take several decades. Such slowly reacting aggregates often exhibit complex mineralogy in which reactive phases are embedded in non-reactive ones.

In order to study the relationship between the progress of ASR and the evolution of the mechanical properties of concrete, a new approach was applied which aims to characterise the advancement of the reaction, from the microstructural point of view, and to relate it to the macroscopic expansion.

Image analysis of BSE images is a powerful tool for characterising concretes. It may be used to measure the degree of hydration and porosity of cement paste [3,4] and also to study the interfacial transition zone between cement paste and aggregate [5]. It is also useful for studying degradation processes [4,6]. It is relatively easy to prepare representative polished sections and to study the alteration at the microscopic level.

Microscopic methods are well established for the diagnosis of the occurrence of ASR. Both optical and electron microscopies have been extensively used to study the occurrence of cracking and gel in aggregates and the surrounding cement paste. Several methods have been studied to estimate the extent of ASR. For instance the concrete surface may be treated with uranyl acetate and fluorescence used to indicate the number of reactive sites [7,8]. Jensen proposed a method based on the number of voids observed in an aggregate to quantify the reaction products in thin sections [9]. Thaulow and Geiker proposed a combined method based on fluorescence thin section petrography, scanning electron microscopy and pore solution expression [10].

The present study concerns the measurement of the extent of ASR, in different aggregates, by image analysis of backscattered electron images (BSE) of polished cross-sections in a scanning electron microscope (SEM). The main objective of

* Corresponding author.
E-mail address: emmanuel.gallucci@epfl.ch (E. Gallucci).

0008-8846/$ - see front matter © 2007 Elsevier Ltd. All rights reserved.
doi:10.1016/j.cemconres.2007.04.016

Table 1
Mixture proportions and curing conditions

	Microbar	Mortar	Concrete
Aggregate size	16–63 μm	0–3 mm	0–15 mm
Cement–aggregate ratio	2, 5, 10	1/3	1/6
Water–cement ratio	0.3	0.51	0.46
Specimen size	10×10×40 mm	40×40×160 mm	70×70×280 mm
Storage temperature	150 °C, autoclave	20, 40, 60 °C	20, 40, 60 °C
Storage time	2 days	2, 23, 40, 90, 180 days	Various
Alkali content	1.5 Na_2O_{eq}	0.8, 1.2	0.4, 0.8, 1.2
Environment	Alkaline environment	Immersed in water	Immersed in water
Tests	SEM-IA expansion	SEM-IA expansion	SEM-IA expansion

this work is to establish a more precise quantitative relationship between the overall expansion of the samples due to the ASR and the degree of the reaction, through a study of laboratory specimens (mortar and concrete) affected by ASR. As a first step, the rather severe "microbar test" which mainly consists in the curing of the prisms for 6 h at 150 °C in alkaline environment was used to quickly obtain aggregates with a high degree of reaction. The "maximum" degree of reaction observed with this method was then compared, in a second step, with the extent of the reaction of the same aggregates in mortar and concrete prisms with different alkaline content, immersed in water at different temperatures.

2. Materials and methods

2.1. Aggregates

Three kinds of aggregates from the Swiss Alps were studied. Petrographic examination showed that aggregate A consisted of layers of chlorite interleaved with layers of quartz and feldspar. Aggregate B was a biotitic schist containing phyllosilicates while aggregate C was biotitic schist with feldspar and some muscovite. Polished samples of all three aggregates were immersed in 2 M NaOH at a temperature of 38 °C for two weeks and then for another week at 50 °C. After this treatment X-ray diffraction indicated that aggregates A and C had undergone significant dissolution, while aggregate B had not.

Mercury intrusion porosimetry (MIP) was conducted on the three aggregates. Three specimens were used for each aggregate. The samples were dried in an oven at a temperature of 105–110 °C for 48 h and stored in a desiccator over silica gel until tested.

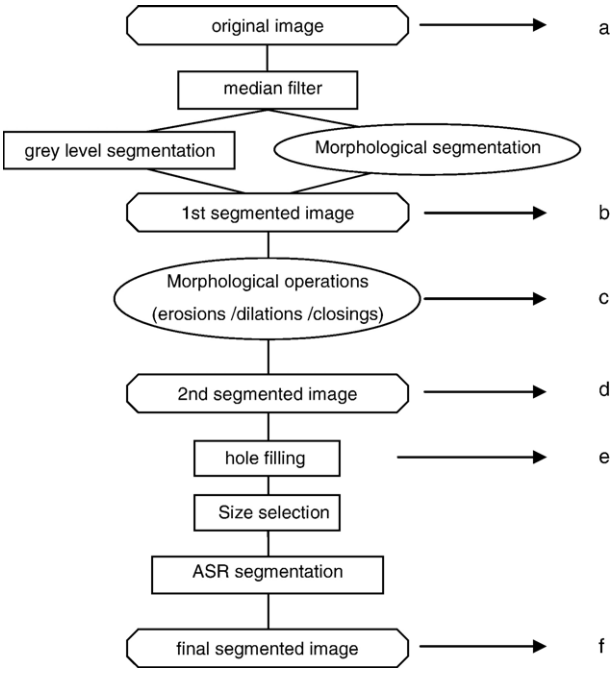

Fig. 2. Image analysis sequence (letters a–f refer to snapshots in Fig. 3).

2.2. Mix proportions and curing regimes

Three types of testing, i.e. microbars, mortar bars and concrete prisms were performed on each aggregate. The

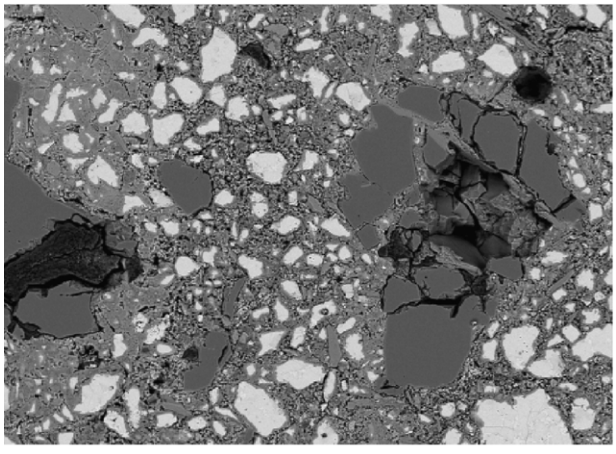

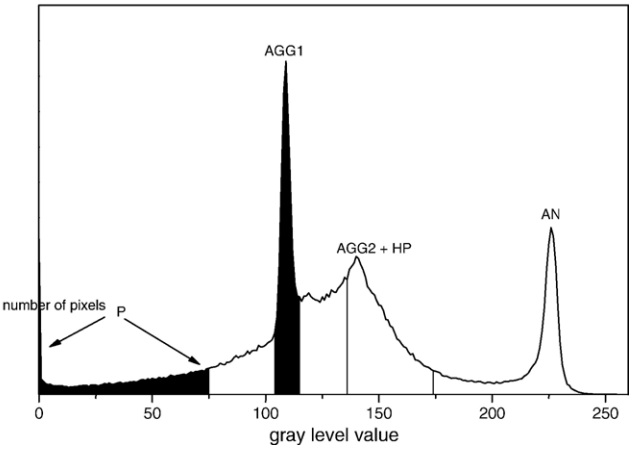

Fig. 1. SEM-BSE image (×200) and corresponding grey level histogram (P = porosity and ASR aggregates, AGGI and AGG2 = aggregate, HP = hydrated products, AN = anhydrous cement grains).

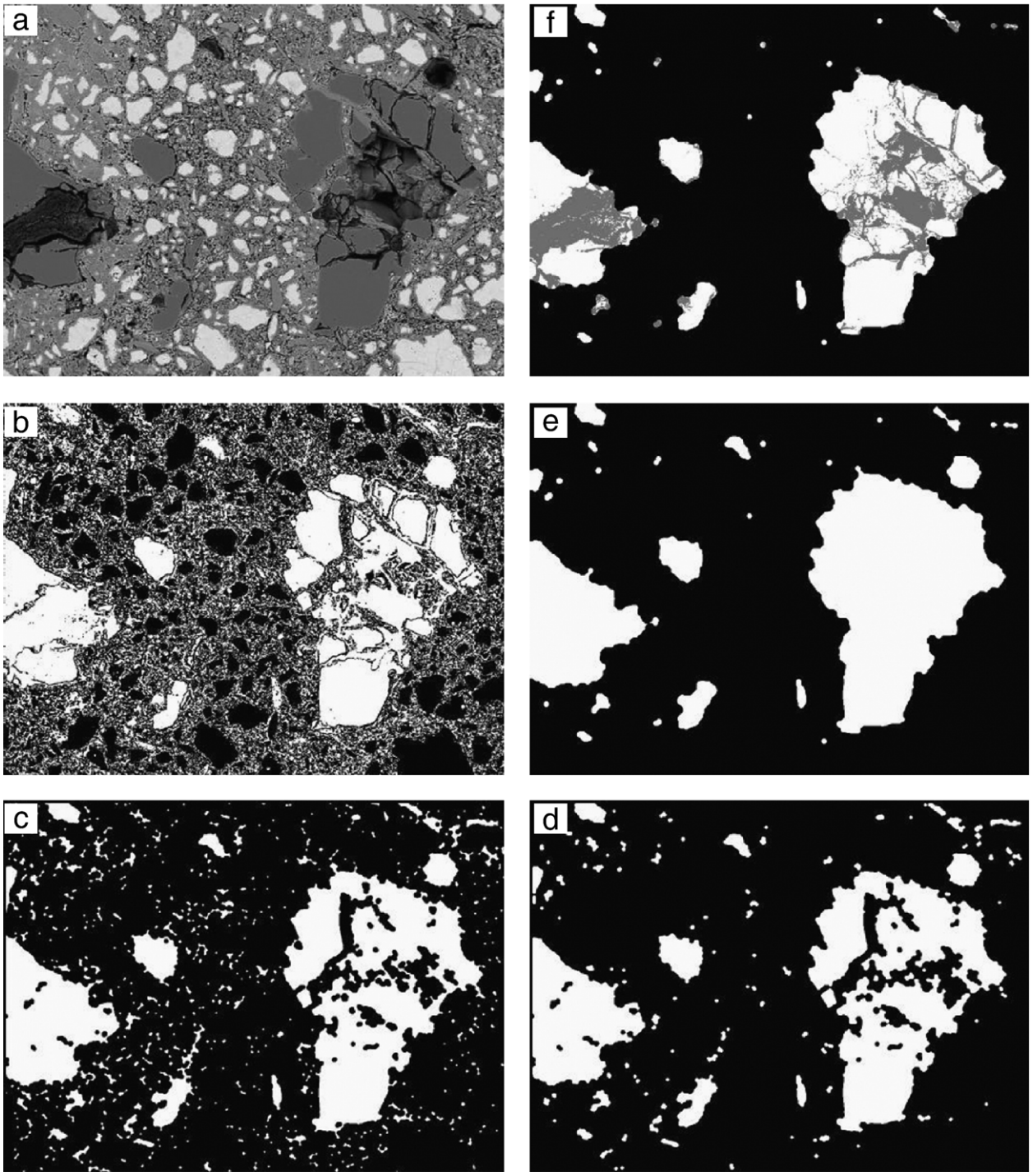

Fig. 3. Snapshots during IA sequence (letters a–f refer to those in Fig. 2).

corresponding mix proportions prepared are summarised in Table 1. In all mixes, the same Portland cement with 0.4% Na_2O_{eq} was used. The effect of the alkali content was studied by increasing known amounts of sodium hydroxide. The microbars were prepared for three cement–aggregate (C/A) ratios 2, 5 and 10 and cured according to the procedures described in the standard test AFNOR XP P 18-594 (24 h of cure in moulds at 20 °C/4 h of steam curing/6 h at 150 °C in alkaline environment/ a few hours at 20 °C). Four bars were subjected to the test and one bar from each batch was cured for 3 days at 20 °C as a reference sample.

The mortar bars (40 × 40 × 160 mm in size) and concrete prisms (70 × 70 × 280 mm in size) were stored at three temperatures 20, 40 and 60 °C. In both cases, extra alkalis in the form of NaOH were added to the mixing water to bring the amount of alkalis to 0.8% and 1.2% Na_2O_{eq} by weight of cement. The samples were demoulded after 24 h and cured at 20 °C in a humid chamber for another 24 h. They were then all

Table 2
Reliability of the image analysis method

Mix design C/A ratio	2		5	
	Experimental volume	Image surfaces	Experimental volume	Image surfaces
Aggregate	38 cm^3	18.75 10^6 px^{-2}	19 cm^3	8.51 10^6 px^{-2}
Total	162 cm^3	78.03 10^6 px^{-2}	174 cm^3	78.03 10^6 px^{-2}
Fraction (%)	23.7	24.03	10.91	10.86

Original porosity of aggregates

	Aggregate A	Aggregate B	Aggregate C
MIP (%)	4.07	1.87	2.07
IA (%)	3.47	1.53	1.83

stored under in separate containers, with a small amount of water to limit the leaching of alkalis — the pH of the storage bath solutions did not significantly change during the experimental period (1 year). The cure under water was chosen to insure a faster reaction and prevent shrinkage. In the other hand, this induces a slight swelling due to the absorption of water, which was considered not significant compared to expansion due to ASR. For each experimental condition 4 bars were prepared : 3 for the measurement of expansion and one from which slices were taken for microscopic analysis.

The axial expansion – perpendicular to casting direction – of each sample was measured at selected ages with comparometer with an accuracy of 0.001 mm and an Invar standard bar as reference. Initial readings were made just before the samples were put in the water. Before all successive measurement, the samples were cooled at 20 °C in the humid chamber for 14 h. As soon as the measurements were completed, the samples were returned to storage box.

2.3. SEM : sample preparation and image analysis

After selected period of time, two slices (between 2 and 5 mm) were cut from one of the samples. For the microbars, specimens were cut in the longitudinal and transverse directions, to verify the statistical isotropy of the samples. The slices

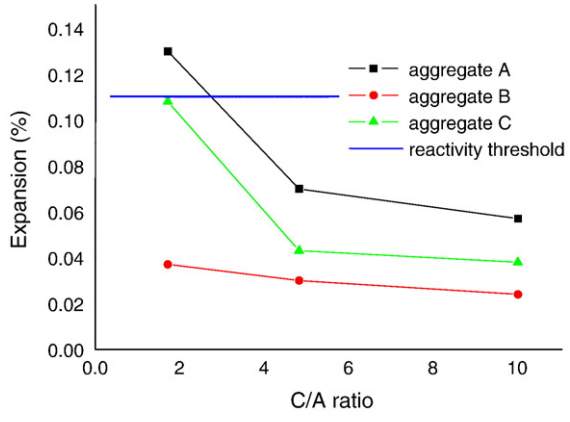

Fig. 4. Expansion of aggregates from microbar tests.

Table 3
Degree of reaction (from IA) of the different aggregates in the microbar test

C/A ratio	Aggregate A (%)	Aggregate B (%)	Aggregate C (%)
2	12.0	5.7	11.6
5	12.4	4.3	11.7
10	12.5	4.3	11.5

The mean error for each sample is ±0.1.

were dried in a vacuum desiccator for 3 days at 20 °C. The microbar reference specimen (not subject to high temperature storage) confirmed that this drying method did not induce any significant cracking in the samples. After drying, the slices were vacuum impregnated with low viscosity resin (EPOTEK 301) and softly polished with decreasing grades of diamond crystallites down to 0.25 μm.

Backscattered electron (BSE) images of the polished sections were acquired using an FEI QUANTA 200 Scanning Electron Microscope. BSE generate a specific phase contrast which allows phases to be identified according to their brightness in the image, those with the greatest average atomic number being the brightest, and those with the lower atomic number being darker. This allows the components of the microstructure to be discriminated on the basis of the grey level histogram of the image (distribution of the grey levels of all pixels of the image). A typical BSE image and its corresponding grey level histogram are given in Fig. 1. The grey level scale extends from black: 0 to white: 255.

Due to their complex mineralogy, there are several ranges of grey levels corresponding to aggregates, which overlap with those of the cementitious phases: between 0 and 75: reacted aggregates and capillary porosity of the cement paste, around 110: silicate aggregates between 135 and 175: wide range of various aggregate minerals (calcium based) but also hydrated cementitious products (mainly CSH).

For isotropic materials (which is the case here since the casting of conventional concrete is not supposed to induce any preferred orientation of any of the constituents/this was checked with analysing perpendicular sections of the same specimens), the oldest and most basic stereological principle states that the surface fraction of a phase in a 2-D image is an unbiased estimate of its volume fraction in the bulk material [11]. The degree of ASR of an aggregate can therefore be simply measured by relating its reacted surface to its total surface in a 2-D cross section. To do this the aggregates must be segmented from the image. In favourable cases, the segmentation can be performed solely on the basis of the grey level. In the present case, because of the high degree of intermixing of grey levels from aggregates and cementitious phases, the extraction of aggregates from the images was based both on grey level and morphological operations (size, shape, homogeneity... of aggregates). Several morphological filters (erosions, dilations, closing...) and other image analysis operations (hole filling...) were applied to the segmented images to improve their reliability. The resultant images consisted only of the aggregates from which it was easy to measure the reacted and non-reacted surfaces. Fig. 2 illustrates the image analysis sequence (which is

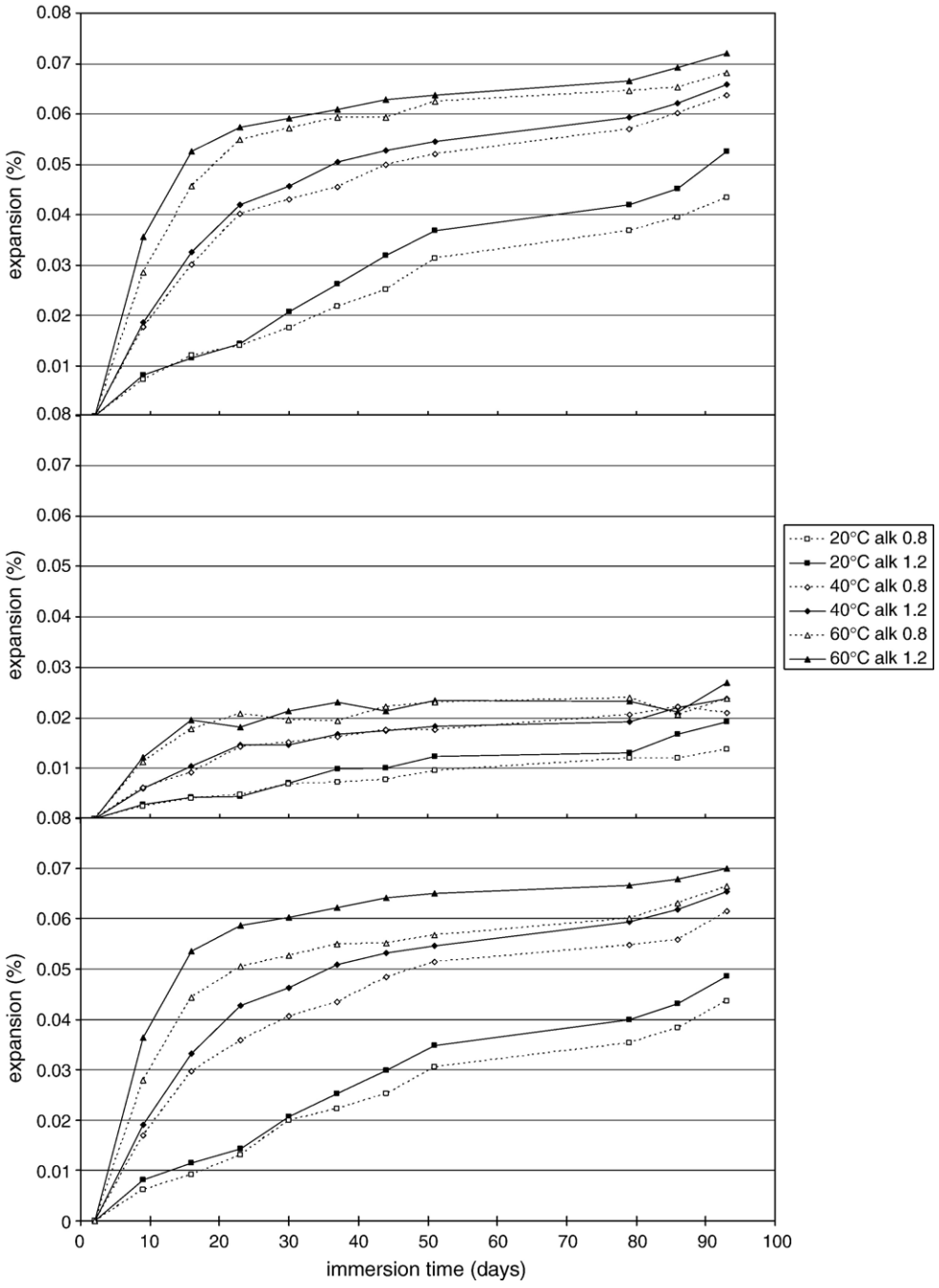

Fig. 5. Expansion of mortar bars under 3 temperatures and 2 alkaline contents.

relatively close to similar methods reported in the literature for these materials, i.e. [12]), while Fig. 3 presents an example of its application to an image.

In this approach, each aggregate in the segmented images is therefore considered as one independent feature from which it is easy to isolate the reacted part (generally dark since it is filled with epoxy) from the rest which remains safe. The ratio between the two surfaces leads to the degree of reaction. Since the microstructure of cementitious materials is heterogeneous at the micron scale, image analysis has to be done on a large number of fields in order to take into account the variation from one field to another. At a magnification of 200× 100 images were found to be sufficient to consider and take into account about 5000 independent aggregates which is large enough to ensure that the results are statistically relevant, as discussed below.

The accuracy of the image analysis (IA) method was checked in two ways:

- comparison of the total amount of aggregate measured by IA and the known volume fraction calculated from the mix design.
- comparison of the porosity measured by IA in the untreated aggregate of the reference microbars (3 days at 20 °C) and the porosity measured by MIP on the as received aggregates.

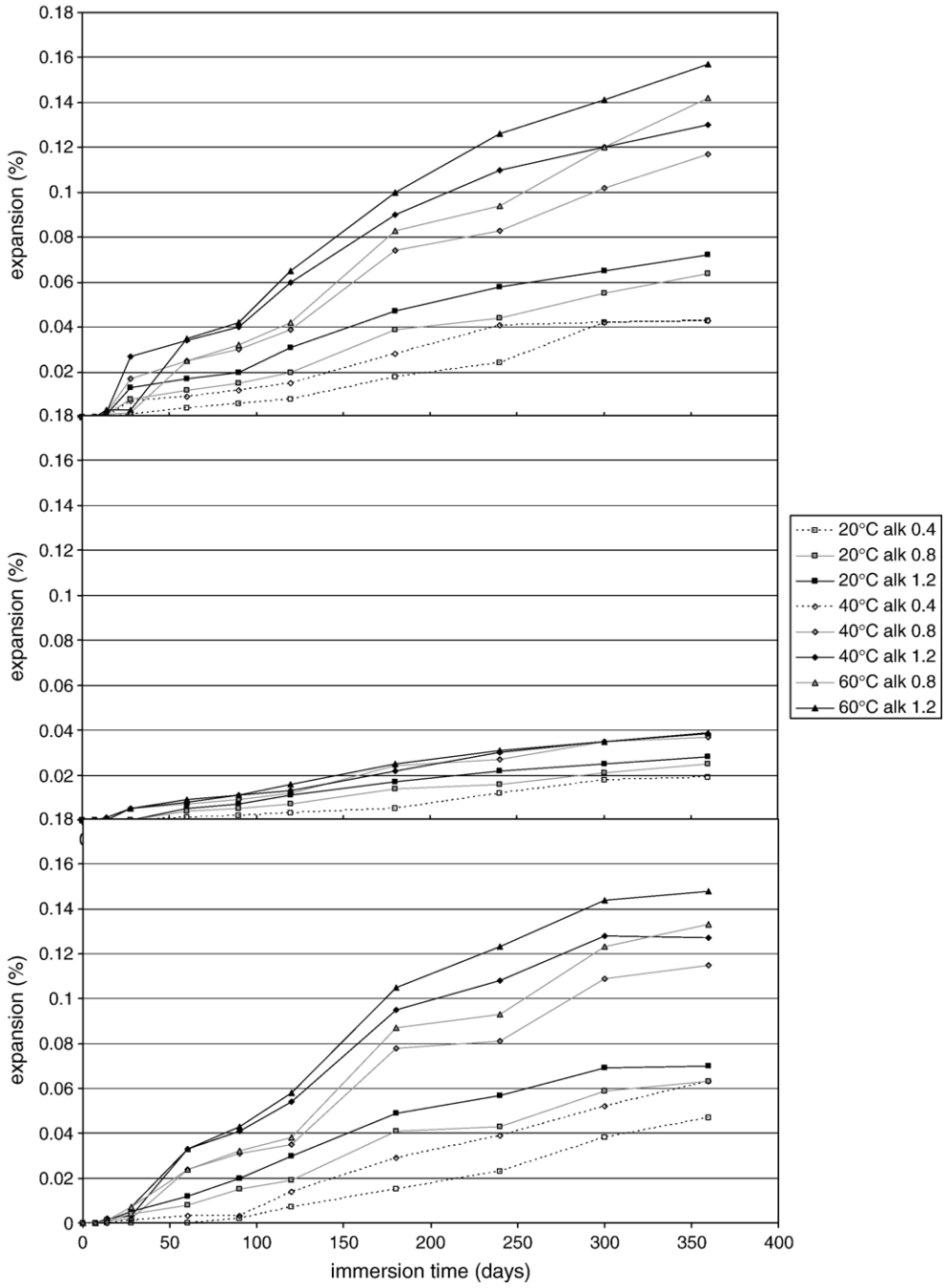

Fig. 6. Expansions of concrete prisms under 3 temperatures and 3 alkali contents.

The results of these comparisons are shown in Table 2. It can be seen there is very good agreement in both cases.

3. Results and discussion

3.1. Microbar test

Fig. 4 shows the expansion of the aggregates in the microbars prepared from the three aggregates for cement–aggregate ratios (C/A) of 2, 5 and 10. As observed in most of the cases, the expansion decreases with increasing C/A ratio. The solid horizontal line at 0.11% indicates the limit recommended by the test as a threshold of reactivity. It can be seen that aggregates A and C would be identified as potentially reactive (especially for lower realistic C/A ratios) while B would be non-reactive.

As seen in Fig. 1, the elevated temperature and alkaline environment of the microbar test led to a high degree of reaction of the reactive aggregates, with the formation of holes and voids within the aggregate particles.

The aforementioned image analysis method was used to quantify the reacted proportion of aggregate during the test. The

Table 4
Reactivity of mortars at different temperatures and alkaline contents

Temperature (°C)	Age (days)	0.8% Na_2O_{eq}			1.2% Na_2O_{eq}		
		Aggregate A (%)	Aggregate B (%)	Aggregate C (%)	Aggregate A (%)	Aggregate B (%)	Aggregate C (%)
20 (leached)	2	0		0	0	0	0
	23				0.24	0.07	0.2
	40	0.34		0.32	0.38	0.15	0.34
	90	0.39		0.35	0.39	0.15	0.35
20 (not leached)	23				0.24		0.2
	40	0.38		0.32	0.39		0.37
	90	0.51		0.41	0.57		0.49
	180	0.64		0.51	0.74		0.68
40	23				0.48	0.14	0.39
	40	1.02	0.2		1.44	0.2	1.07
	90	1.45		1.28	1.95	0.21	1.78
	180	1.87		1.81	2.07	0.22	1.91
60	23				0.84	0.17	0.61
	40	2.01	0.22		3.01	0.22	2.06
	90	2.85		2.15	3.04	0.21	2.08
	180	3.09	0.34	2.75	3.09	0.23	2.15

results presented in Table 3 show that the microbar test induces a very high reaction degree. For the aggregates A and C, classed as potentially reactive, the ultimate reaction degree is around 12% and only 5% for the aggregate B classed non-reactive. The values are independent of the C/A ratio, this is expected as there is an excess of alkali supplied to the specimens in this test so there is no reason that the chemical reaction should depend on the ratio of cement to aggregate. It should be noted that at such high temperatures even crystalline quartz will show some reaction, therefore the degrees of reaction obtained in this test will be much higher than those expected at more realistic temperatures and should be considered as the very ultimate possible degree of reaction which could be observed in the studied aggregates.

3.2. Expansion of mortar and concrete prisms

Fig. 5 and Fig. 6 show the expansion of the mortar and concrete samples respectively. Each value is the average of axial readings on three samples. The samples were prepared from the three aggregate types exposed at different temperatures and alkali contents. Expansion levels were different due to the reactivity of aggregates, to the temperature level and the alkali content of the mixtures. The results are consistent with those found in the microbar test; where aggregates A and C show significant reaction while aggregate B exhibits a lower reactivity.

Mortar bars made with aggregates A and C show large expansions (at the two higher temperatures after only 20 to 40 days, while those made with aggregate B remains low at all temperatures. Results on concrete samples show the same trends with respect to aggregate, temperature and alkali level as the mortar samples but with a lower expansion rate (because of coarser aggregates) and higher expansion values (because of larger aggregate content).

At 60 °C the maximum expansion levels of the mortar bars, reached at about 90 days, were 0.065% for aggregate C, 0.06% for aggregate A and 0.025% for aggregate B. For concrete prisms the maximum expansion levels are reached only after more than 350 days at 60 °C and were 0.16% aggregate A, 0.15% for aggregate A and 0.03% for aggregate B. However, both the mortar and concrete prisms made with aggregate B have the same expansion even though the concretes have nearly twice the aggregate content. This indicates that the expansion of specimens made of aggregate B may be attributed to normal expansion under water and not to ASR. This result is in accordance with many results in the literature for non-reactive aggregates [13,14].

Table 5
Reactivity of concrete at different temperatures and different alkaline contents

Alkalinity	Age (days)	Aggregate A (%)			Aggregate C (%)		
(Na_2O_{eq})		20 °C	40 °C	60 °C	20 °C	40 °C	60 °C
0.4	60						
	120		0.153	0.212		0.143	0.224
	300		0.238			0.304	
0.8	60						
	120						0.270
	300	0.612		2.520	0.612	1.940	2.220
1.2	60		0.347			0.260	0.371
	120			1.571			
	300		2.104	2.201		2.504	2.601

3.3. Degree of reaction of mortar and concrete prisms

Polished sections were prepared from the mortar bars at 2, 23, 40, 90 and 180 days and the degree of reaction of the aggregates was measured by the image analysis method. The results for the mortars with alkali content of 1.2 and 0.8 are shown in Table 4 (not all samples showing low degree reaction – especially those made with aggregate B – were analysed). It is observed that the maximum amount of reaction in the mortar bars at the plateau of expansion is much lower (3% for

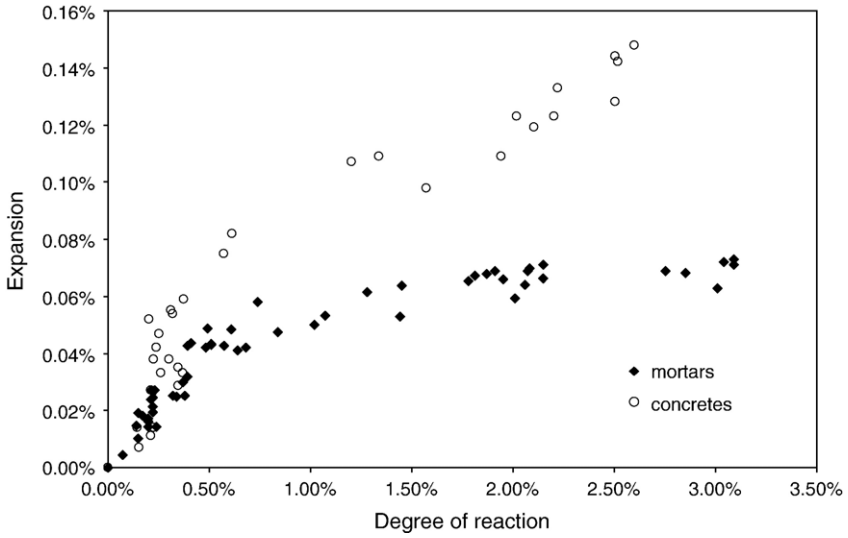

Fig. 7. Expansions vs. observed reactivity of all mortars and concrete samples.

aggregates A and C, and 0.25% for aggregate B) than that observed in the microbar test (12% aggregates A and C, and 5% for aggregate B).

The reactivity of concrete samples at different time intervals is given in Table 5. The samples from aggregate B did not expand significantly. For this reason the measurements were limited to the two reactive aggregates A and C. Image analysis was performed when changes in expansion and other mechanical properties were observed. From Table 5, the limits of reaction of the concrete are similar to those observed in mortars, but are reached at longer times. The ultimate degree of reaction obtained at 40 and 60 °C at the two high alkaline compositions are almost the same 2.6% and 2.2% for concretes A and C respectively, compared with 3.0% and 2.2% in the mortar bars from the same aggregates. Thus, theses results confirm those obtained on the microbar samples, regarding the independence of the reaction degree from the C/A ratio.

4. Discussion

In the previous section, both expansion measurements and calculation of degree of reaction were performed in parallel for all mortar and concrete samples. The expansion is measured is the apparent macroscopic manifestation of the ASR while the degree of reaction is an indicator of ASR at the microstructural level. Fig. 7 presents the relationships obtained between the expansion and the degree of reaction for both mortar and concrete samples. The results show a strong correlation between the expansion and the degree of reaction: for each type of specimen (concrete or mortar), all the points seem to belong

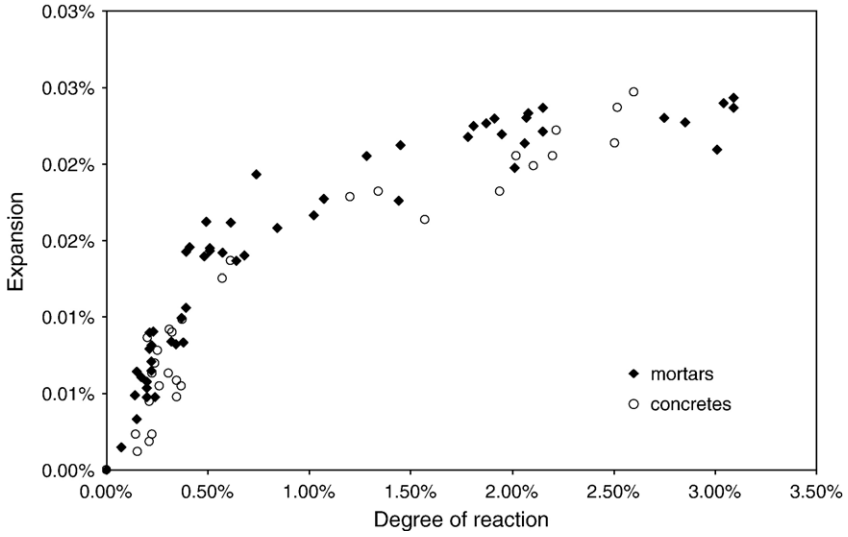

Fig. 8. Expansions normalised to C/A = 1 vs. observed reactivity.

to a same 'master curve' whatever the aggregate type (A, B or C), the temperature or the alkali content. The predominant factor seems to be the cement to aggregate (C/A) ratio as shown in the normalised curve presented in Fig. 8. A linear domain is observed – which corresponds to a constant expansion rate in terms of degree of reaction – up to approximately a reaction degree of 0.3% followed by wider non-linear domain. At this critical degree of reaction, the average corresponding expansion is around 0.03% and 0.06% for mortar and concrete samples respectively. Beyond this critical value, the expansion rate decreases as the ASR induced cracking starts to develop mainly within the aggregates since very few cracks are observed within the matrix at this stage of the study (Fig. 1). At later stages of expansion, the cracks may obviously propagate into the matrix phase. Moreover, it should be stated that these critical expansion values for mortar and concrete are larger than the intrinsic strain limit of the aggregates which lay between 0.016% and 0.018%. This additional expansion corresponds to the contribution of the matrix and the pre-existing microcracks to the overall ductility of the material.

5. Conclusion

The BSE image technique offers an objective and reliable method to quantifying the reactivity of the aggregates. The results presented here show that there is good correlation between the progress of the ASR as measured by microscopy and the macroscopic expansion. This relationship depends only on the formulation of the cementitious material (cement–aggregate ratio and the particle size of aggregate) and not on the kinetics of the reaction i.e. it seems to be independent from temperature and alkali content. This method is a promising tool for a quantitative assessment of the expansion related to ASR, however only limited number of aggregate types were studied, so these findings cannot be generalized at this stage.

References

[1] D.W. Hobbs, Influence of mix proportions and cement alkali content upon expansion due to the alkali-silica reaction, Technical Report — Cement and Concrete Association 534 (1980).
[2] R. Narayan Swamy, M.M. Al-Asali, Expansion of concrete due to alkali-silica reaction, ACI Mater. J. 85 (1) (1988) 33–40.
[3] K.L. Scrivener, H.H. Patel, P.L. Pratt, L.J. Parrott, Analysis of phases in cement paste using backscattered electron images, methanol adsorption and thermogravimetric analysis, Microstructural Development During the Hydration of Cement, Proc. Mat. Res. Soc. Symp. (1987) 67–76.
[4] K.L. Scrivener, Backscattered electron imaging of cementitious microstructures: understanding and quantification, Cem. Concr. Compos. 26 (8) (2004) 935–945.
[5] K.L. Scrivener, E.M.G., Microstructure gradient in cement paste around aggregate in particles, bonding in cementitious composites, in: S. Mindess, S.P. Shah (Eds.), Mater. Res. Soc. Symp. Proc., Pittsburgh, vol. 114, 1988, pp. 77–86.
[6] A.K. Crumbie, K.L. Scrivener, P.L. Pratt, The relationship between the porosity and permeability of the surface layer of concrete and the ingress of aggressive ions, Pore Structure and Permeability of Cementitious Materials, Proc. Mat. Res. Soc. Symp. (1989) 279–284.
[7] K. Natesayier, a.H.K.C., In situ identification of ASR products in concrete, Cem. Concr. Res. 18 (1988) 455–463.
[8] S. Guedon, F. Martineau, Mise en évidence d'un gel d'alcali réaction par flurescence dans un béton agé d'un an, Bulletin de liaison LCPC 175 (1991) 100–101.
[9] Jensen, V., Alkali aggregate reaction in southern Norway. PhD Thesis, 1993. University of Trondheim: p. 262.
[10] Niels Thaulow, Mette Geiker, Determination of the residual reactivity of alkali silica reaction in concrete, 9th International Conference on Alkali Aggregate Reaction in Concrete, vol. 2, 1992, pp. 1050–1058.
[11] A. Delesse, Pour déterminer la composition des roches, Annales des Mines 13 (1848) 379 (fourth series).
[12] R. Yang, N.R. Buenfeld, Binary segmentation of aggregate in SEM image analysis of concrete, Cem. Concr. Res. 31 (3) (2001) 437–441.
[13] S. Fan, J.M. Hanson, Length expansion and cracking of plain and reinforced concrete prisms due to alkali-silica reaction, ACI Mater. J. 95 (4) (1998) 480–487.
[14] N. Smaoui, et al., Evaluation of the expansion attained to date by concrete affected by alkali-silica reaction. Part I: experimental study, Can. J. Civ. Eng. 31 (5) (2004) 826–845.